STRIPE NOISE REMOVAL OF REMOTE SENSING IMAGE WITH A DIRECTIONAL ℓ_0 SPARSE MODEL

Hong-Xia Dou, Ting-Zhu Huang, Liang-Jian Deng, Yong Chen

School of Mathematical Sciences, University of Electronic Science and Technology of China, China

ABSTRACT

This paper commits to remove the stripe noise to enhance the visual quality of remote sensing images, in the meanwhile preserves image details of stripe-free regions. Instead of solving the underlying image as most of researches, we propose a non-convex ℓ_0 model for remote sensing image destriping by taking full consideration of the intrinsically directional and structural priors of stripe noise. Moreover, the proposed non-convex model can be solved by the proximal alternating direction method of multipliers (PADMM) method which theoretically guarantees converging to a KKT point. Extensively experimental results on simulated and real data demonstrate that the proposed method outperforms recent state-of-the-art destriping methods, both visually and quantitatively.

1. INTRODUCTION

Stripe noise (all denoted as ''stripes" in this paper), which has strongly directional and structural information (*e.g.,* pixels damaged on row by row or column by column), generally results in a bad influence not only on visual quality but also on subsequent applications of remote sensing images. There are various kinds of stripes, such as puss-broom [1] and cross-track imaging devices [2], caused by the inconsistence of the detecting element scanning or the influence of the detector moving and temperature changes, *etc*. Therefore, it is necessary to remove the stripes and simultaneously maintain the healthy pixels from degraded images.

Recently, many approaches for destriping problems have been proposed, which may be roughly divided into three categories. The first category is filtering-based methods which are simplicity and have been widely utilized for remote sensing image destriping. These methods will inevitably damage image structures as well as even may generate serious blurring and ringing artifacts with images. Although recently filtering-based methods have improved results, there still exist the mentioned limitations. The second category is statistics-based methods, *e.g.,* [3, 4, 5], which may obtain better results by formulating excellent priors of stripes. However, when the stripes are irregular, the performance of these methods will be unstable. The third category is optimization-based methods that play an important role in image destriping problems. The aim of these methods is to utilize regularization technique to recover the underlying image. In [6], Shen and Zhang have proposed a maximum a posteriori (MAP) framework based on Huber-Markov variational distribution. In [7], the authors present the unidirectional total variational (UTV) model and design a sophisticated algorithm. Furthermore, based on the low-rank prior of stripes, the authors in [8] and [9] have proposed a low-rank prior based model for the destriping applications in hyperspectral images. Most of these works only focus on the various characters of remote sensing images not on the latent properties of stripes which may destroy image details, *e.g.,* sharp image edges. Recently, some state-of-the-art destriping methods utilize latent properties of stripes to get perfect performance on stripes removal, *e.g.,* directional and sparse priors in [10] and low-rank prior in [11]. In addition, Yuan *et al.* [12] proposed a ℓ_0 based sparse model for impulse noise removal of nature images, and generate excellent results. However, this method needs to predefine the locations of missing pixels, thus it is not fit with the destriping application of remote sensing images.

In this paper, according to a comprehensive analysis and considering both the directional and sparse properties of stripes, we propose a ℓ_0 sparse model to remove stripes of remote sensing images without location information of stripes. In addition, we employ the PADMM algorithm to solve the proposed non-convex sparse model, which theoretically guarantees convergence to a KKT point. Quantitative and visual results demonstrate the superiority and the stability of the proposed method. In particular, the contributions of the proposed method are summarized as follows: 1) Fully considering the latent priors of stripes, we formulate a ℓ_0 sparse model which can accurately depict the intrinsic sparse character; 2) We solve the proposed non-convex model by a designing PADMM algorithm that theoretically guarantees the convergence; 3) The proposed method, which is not sensitive to related parameters, outperforms recently several state-of-the-art image destriping methods, GSLV [10], LRSID [11], *etc*.

The outline of this paper is organized as follows. In section 2, we present our optimization method which includes the proposed model and the solution. In section 3, experimental results will be exhibited to demonstrate the effectiveness of our method. Finally, we will draw conclusions in section 4.

2. THE PROPOSED METHOD

2.1. The formulation of destriping problem

The stripes mainly includes two types, *i.e.*, additive noise and multiplicative noise. However, the multiplicative noise can be described as additive one by the logarithm. Therefore, researchers more focus on the additive model which is generally described as follows

$$\mathbf{b} = \mathbf{u} + \mathbf{s}, \tag{1}$$

where $\mathbf{b}, \mathbf{u}, \mathbf{s} \in \mathbb{R}^n$ represent the vector forms of the observed image, the underlying image and stripes, respectively. The purpose of our work is to found a reasonable model that is based on the relation (1) and latent priors to estimate the stripes $\mathbf{s}$, then employ the formulation $\mathbf{u} = \mathbf{b} - \mathbf{s}$ to compute the final destriped image $\mathbf{u}$.

2.2. The proposed model

Without loss of generality, here we assume that the stripes is along the y-axis of image. Due to the directional property of stripes, the derivation along y-axis of stripes $\nabla_y \mathbf{s}$ can be viewed as sparse. In addition, the stripes $\mathbf{s}$ also can be assumed as a sparse one, since the stripes in the image is generally not abundant. Furthermore, inspired by the work of UTV, the variational information across stripes direction (*i.e.*, $\nabla_x \mathbf{u}$) is utilized to describe the discontinuity of underlying image. Similar to the work of Chang *et al.* [11], the stripes with original intensity [0, 255] are normalized between [0, 1] for the simplicity of parameter tuning. By the above analysis and the relation $\mathbf{u} = \mathbf{b} - \mathbf{s}$, we finally formulate the non-convex sparse model as follows

$$\min_{\mathbf{s}} \ ||\nabla_y \mathbf{s}||_0 + \mu||\mathbf{s}||_1 + \lambda||\nabla_x(\mathbf{b} - \mathbf{s})||_1, \tag{2}$$

where μ and λ are two positive parameters. Note that here we use ℓ_0 regularizer for $\nabla_y \mathbf{s}$ and ℓ_1 regularizer for $\mathbf{s}$ and $\nabla_x(\mathbf{b} - \mathbf{s})$, since the $\nabla_y \mathbf{s}$ is actually more sparse than $\mathbf{s}$. However, ℓ_0 norm is non-convex and it is not easy to solve the given model if there exist two more ℓ_0 terms (*e.g.,* the convergence and the solution). Therefore, here we only employ one ℓ_0 regularization term which can still promise excellent results.

2.3. The solution of the proposed model

To solve the proposed ℓ_0 sparse model, we introduce the following MPEC (Mathematical Program with Equilibrium Constraints) optimization reformulation which is proposed by Yuan *et al.* [12] to equivalently replace the ℓ_0 term, then employ a PADMM based method to solve the equivalent model. Actually, PADMM based method is an extended version of ADMM method, which has been applicated to many image applications, *e,g.,* image deblurring [13, 14, 15, 16], image super-resolution [17, 18], image unmixing [19] *etc*.

Lemma 1 (MPEC reformulation [12]) *For any given* $\mathbf{w} \in \mathbb{R}^n$*, it holds that*

$$||\mathbf{w}||_0 = \min_{\mathbf{0} \le \mathbf{v} \le \mathbf{1}} \langle \mathbf{1}, \mathbf{1} - \mathbf{v} \rangle, \ s.t., \ \ \mathbf{v} \odot |\mathbf{w}| = 0. \tag{3}$$

where $\odot$ *denotes an elementwise product, and* $\mathbf{v}^* = \mathbf{1} - sign(|\mathbf{w}|)$ *is the unique optimal solution of the minimization problem (3).*

By Lemma 1, our ℓ_0 destriping model (2) is equivalent to the following constraint problem,

$$\begin{aligned} \min_{\mathbf{0} \le \mathbf{V}, \mathbf{s} \le \mathbf{1}} & \langle \mathbf{1}, \mathbf{1} - \mathbf{V} \rangle + \mu||\mathbf{s}||_1 + \lambda||\nabla_x(\mathbf{b} - \mathbf{s})||_1 \\ & s.t. \ \mathbf{V} \odot |\nabla_y \mathbf{s}| = 0. \end{aligned} \tag{4}$$

According to the analysis of [12], if $\mathbf{s}^*$ is the globally unique minimization solution of Eq. 2, then $(\mathbf{s}^*, 1 - \text{sign}(|\nabla_y \mathbf{s}^*|))$ is the globally unique minimization solution of Eq. 4. Making variable substitutions for the ℓ_1 norm in (4), *i.e.*, $\mathbf{H} = \nabla_y \mathbf{s}$, $\mathbf{Z} = \mathbf{s}$ and $\mathbf{W} = \nabla_x(\mathbf{b} - \mathbf{s})$, the augmented Lagrangian function $\mathcal{L}$ is as follows

$$\begin{aligned} & \mathcal{L}(\mathbf{H}, \mathbf{Z}, \mathbf{W}, \mathbf{V}, \mathbf{s}, \boldsymbol{\pi}_1, \boldsymbol{\pi}_2, \boldsymbol{\pi}_3, \boldsymbol{\pi}_4) \\ & = \langle \mathbf{1}, \mathbf{1} - \mathbf{V} \rangle + \mu||\mathbf{Z}||_1 + \lambda||\mathbf{W}||_1 + \langle \nabla_y \mathbf{s} - \mathbf{H}, \boldsymbol{\pi}_1 \rangle \\ & + \frac{\beta_1}{2}||\nabla_y \mathbf{s} - \mathbf{H}||^2 + \langle \mathbf{s} - \mathbf{Z}, \boldsymbol{\pi}_2 \rangle + \frac{\beta_2}{2}||\mathbf{s} - \mathbf{Z}||^2 \\ & + \langle \nabla_x(\mathbf{b} - \mathbf{s}) - \mathbf{W}, \boldsymbol{\pi}_3 \rangle + \frac{\beta_3}{2}||\nabla_x(\mathbf{b} - \mathbf{s}) - \mathbf{W}||^2 \\ & + \langle \mathbf{V} \odot |\mathbf{H}|, \boldsymbol{\pi}_4 \rangle + \frac{\beta_4}{2}||\mathbf{V} \odot |\mathbf{H}||^2, \end{aligned} \tag{5}$$

where $\boldsymbol{\pi}_1, \boldsymbol{\pi}_2, \boldsymbol{\pi}_3$ and $\boldsymbol{\pi}_4$ are Lagrange multipliers, and $\beta_1, \beta_2, \beta_3$ and β_4 are positive parameters. The minimization problem Eq. 5 can be solved by PADMM based algorithm. Next, we discuss the solution of each subproblem.

a) Here, PADMM algorithm needs to introduce a convex proximal term $\frac{1}{2}||\mathbf{s} - \mathbf{s}^k||_D^2$, then the $\mathbf{s}$-subproblem becomes a strong convex optimization

$$\begin{aligned} \min_{\mathbf{0} \le \mathbf{s} \le \mathbf{1}} \ & \langle \nabla_y \mathbf{s} - \mathbf{H}^k, \boldsymbol{\pi}_1^k \rangle + \frac{\beta_1}{2}||\nabla_y \mathbf{s} - \mathbf{H}^k||^2 \\ & + \langle \mathbf{s} - \mathbf{Z}^k, \boldsymbol{\pi}_2^k \rangle + \frac{\beta_2^k}{2}||\mathbf{s} - \mathbf{Z}^k||^2 \\ & + \langle \nabla_x(\mathbf{b} - \mathbf{s}) - \mathbf{W}^k, \boldsymbol{\pi}_\mathbf{3}^k \rangle \\ & + \frac{\beta_3^k}{2}||\nabla_x(\mathbf{b} - \mathbf{s}) - \mathbf{W}^k||^2 + \frac{1}{2}||\mathbf{s} - \mathbf{s}^k||_D^2, \end{aligned} \tag{6}$$

where

$$D = \frac{1}{\kappa} I - (\beta_1 \nabla_y^T \nabla_y + \beta_2 + \beta_3 \nabla_x^T \nabla_x),$$

$$\kappa \in \left(0, \frac{1}{\beta_1 ||\nabla_y||^2 + \beta_2 + \beta_3 ||\nabla_x||^2}\right).$$

Then, the $\mathbf{s}$-subproblem holds the following closed-form solution,

$$\mathbf{s}^{k+1} = \min(\mathbf{1}, \max(\mathbf{0}, \mathbf{g}^k)). \tag{7}$$

where $\mathbf{g}^k = \mathbf{s}^k - \kappa[\beta_1(\nabla_y \mathbf{s}^k - \mathbf{H}) + \beta_2(\mathbf{s}^k - \mathbf{Z}) - \beta_3 \nabla_x^T(\nabla_x \mathbf{b} - \nabla_x \mathbf{s}^k - \mathbf{W})]$.

b) The $\mathbf{H}$-subproblem can be rewritten as the following minimization problem,

$$\begin{aligned}\min_{\mathbf{H}} \ &\langle \nabla_y \mathbf{s}^{k+1} - \mathbf{H}, \boldsymbol{\pi}_1^k \rangle + \frac{\beta_1}{2} ||\nabla_y \mathbf{s}^{k+1} - \mathbf{H}||^2 \\ &+ \langle \mathbf{V}^k \odot |\mathbf{H}^k|, \boldsymbol{\pi}_4^k \rangle + \frac{\beta_4}{2} ||\mathbf{V}^k \odot |\mathbf{H}^k|||^2,\end{aligned} \tag{8}$$

if $\mathbf{H} > 0$,

$$\mathbf{H}^{k+1} = \frac{(\beta_1 \nabla_y \mathbf{s}^{k+1} + \boldsymbol{\pi}_1^k) - \boldsymbol{\pi}_4^k \odot \mathbf{V}^k}{\beta_1 + \beta_4 \mathbf{V}^k \odot \mathbf{V}^k}, \tag{9}$$

if $\mathbf{H} < 0$,

$$\mathbf{H}^{k+1} = (-1)\frac{-(\beta_1 \nabla_y \mathbf{s}^{k+1} + \boldsymbol{\pi}_1^k) - \boldsymbol{\pi}_4^k \odot \mathbf{V}^k}{\beta_1 + \beta_4 \mathbf{V}^k \odot \mathbf{V}^k}. \tag{10}$$

In summary, the $\mathbf{H}$-subproblem has the following closed-form solution,

$$\mathbf{H}^{k+1} = \text{sign}(\mathbf{q}^k) * \frac{|\mathbf{q}^k| - \boldsymbol{\pi}_4^k \odot \mathbf{V}^k}{\beta_1 + \beta_4 \mathbf{V}^k \odot \mathbf{V}^k}, \tag{11}$$

where $\mathbf{q}^k = \beta_1^k \nabla_y \mathbf{s}^{k+1} + \boldsymbol{\pi}_1^k$

c) The $\mathbf{Z}$-subproblem is given as follows,

$$\min_{\mathbf{Z}} \ \mu||\mathbf{Z}||_1 + \langle \mathbf{s}^{k+1} - \mathbf{Z}, \boldsymbol{\pi}_2^k \rangle + \frac{\beta_2^k}{2} ||\mathbf{s}^{k+1} - \mathbf{Z}||^2, \tag{12}$$

which has closed-form solution by soft-thresholding strategy [20]

$$\mathbf{Z}^{k+1} = \mathbf{Shrink}(\mathbf{s}^{k+1} + \frac{\boldsymbol{\pi}_2^k}{\beta_2^k}, \frac{\mu}{\beta_2^k}), \tag{13}$$

where $\mathbf{Shrink}(\mathbf{a}, \mathbf{T}) = \text{sign}(\mathbf{a}) * \max(|\mathbf{a} - \mathbf{T}|, 0)$.
d) Similar to $\mathbf{Z}$-subproblem, $\mathbf{W}$-subproblem has the following closed-form solution by soft-thresholding strategy,

$$\mathbf{W}^{k+1} = \mathbf{Shrink}(\mathbf{q}^k, \frac{\lambda}{\beta_3^k}), \tag{14}$$

where $\mathbf{q}^k = \nabla_x(\mathbf{b} - \mathbf{s}^{k+1}) + \frac{\boldsymbol{\pi}_3^k}{\beta_3^k}$.

e) The $\mathbf{V}$-subproblem can be written as follows,

$$\min_{\mathbf{0}<\mathbf{V}<\mathbf{1}} \ \langle \mathbf{V}, \mathbf{c}^k \rangle + \frac{\beta_4}{2} ||\mathbf{V} \odot |\mathbf{H}^{k+1}|||^2, \tag{15}$$

where $\mathbf{c}^k = \mathbf{1} - \boldsymbol{\pi}_4^k \odot |\mathbf{H}^{k+1}|$. By least squares method and the nonnegative constrain $\mathbf{0} < \mathbf{V} < \mathbf{1}$, it has the closed-form solution,

$$\mathbf{V}^{k+1} = \min\left(\mathbf{1}, \max\left(\mathbf{0}, \frac{\mathbf{c}^k}{\beta_4 |\mathbf{H}^{k+1}| \odot |\mathbf{H}^{k+1}|}\right)\right). \tag{16}$$

f) Finally, we update the Lagrange multipliers by

$$\begin{aligned}\boldsymbol{\pi}_1^{k+1} &= \boldsymbol{\pi}_1^k + \beta_1(\nabla_y \mathbf{s}^{k+1} - \mathbf{H}^{k+1}), \\ \boldsymbol{\pi}_2^{k+1} &= \boldsymbol{\pi}_2^k + \beta_2(\mathbf{s}^{k+1} - \mathbf{Z}^{k+1}), \\ \boldsymbol{\pi}_3^{k+1} &= \boldsymbol{\pi}_3^k + \beta_3(\nabla_x(\mathbf{b} - \mathbf{s}^{k+1}) - \mathbf{W}^{k+1}), \\ \boldsymbol{\pi}_4^{k+1} &= \boldsymbol{\pi}_4^k + \beta_4(\mathbf{V}^{k+1} \odot |\mathbf{H}^{k+1}|).\end{aligned} \tag{17}$$

Combining **step a)** to **step f)**, we formulate the final algorithm to iteratively solve the proposed ℓ_0 sparse model (2) with the initial guesses $\mathbf{s}^0 = \mathbf{b}$, $\boldsymbol{\pi}_i^0 = 0, i = 1, \cdots, 4$, $\mathbf{H}^0 = \mathbf{Z}^0 = \mathbf{W}^0 = \mathbf{0}$. Moreover, the algorithm guarantees the convergence to a KKT point.

3. EXPERIMENT RESULTS

In this paper, we compare the proposed method with several state-of-the-art image destriping methods, including the statistical linear destriping (SLD) [1], the unidirectional total variation model (UTV) [7], the global sparsity and local variational (GSLV) [10], and the low-rank single-image decomposition (LRSID) [11]. For the simulated experiments, we add the period and non-period stripes with intensity [0,1] to the underlying images, respectively, then apply different methods to compare the performance. All experiments are conducted in MATLAB (R2016a) on a desktop with 16Gb RAM and Inter(R) Core(TM) CPU i5-4590: @3.30GHz.

For the parameters, we empirically set $\lambda = 10$, $\mu = 1$ and $\beta_i = 1, i = 1, 2, 3, 4$. Note that although fine tuning of parameters can get better results, we unify the parameter selection to show the stability of the proposed method. The parameters of comparing methods are set according to the default or suggested parameters in their papers and codes. Furthermore, we also employ some acknowledged indexes, i.e., peak signal-to-noise ratio (PSNR) and structural similarity index (SSIM) [21], to evaluate the performance of different methods. For the convenient and uniform comparisons, all test images are normalized to [0,1].

Table 1 reports the averagely quantitative comparisons on 32 remote sensing images[1] with simulated period (Per) and non-period (NonPer) stripes, which the stripes is mainly determined by noise ration r and added stripe "Intensity". From the table, we know that the proposed method obtains the best PSNR and SSIM performance. Although the standard deviations of PSNR are not the smallest, the standard deviations of SSIM hold the best performance, which indicates our method performs more stable on structural similarity.

Fig. 1 presents visual results of real data with stripes of unknown type. From the figure, the proposed method not only removes the stripes completely, but also preserves image details of stripe-free regions well. In particular, the comparing

[1]From "DigitalGlobe" with randomly selecting 32 images: `https://www.digitalglobe.com/product-samples`

Table 1. Averagely quantitative comparisons on 32 images with simulated Per noise and NonPer noise (Bold: the best).

	Stripe type	Per noise				NonPer noise			
		Intensity = 50/255		Intensity = 100/255		Intensity = 50/255		Intensity = 100/255	
Index	Method	r = 0.2	r = 0.6	r = 0.2	r = 0.6	r = 0.2	r = 0.6	r = 0.2	r = 0.6
PSNR	SLD [1]	41.710±2.93	41.957±2.928	40.614±2.549	41.644±2.836	35.964±1.510	42.007±3.020	30.963±1.414	28.403±1.729
	UTV [7]	40.920±2.773	43.086±2.298	41.470±3.385	41.058±3.299	35.648±1.527	42.505±3.010	31.055±4.687	31.599±2.578
	GSLV [10]	40.202±3.058	39.962±2.856	40.168±3.091	39.044±2.705	41.985±1.239	39.838±2.903	41.684±1.399	35.408±2.472
	LRSID [11]	40.308±2.169	40.548±1.976	39.642±2.500	41.035±2.014	43.001±1.349	40.497±2.024	37.779±1.212	33.559±1.132
	Proposed	**52.853±4.910**	**49.212±4.390**	**52.854±4.902**	**49.182±4.368**	**49.057±4.791**	**49.057±4.492**	**44.365±5.106**	**39.452±4.494**
SSIM	SLD [1]	0.9965±0.003	0.9965±0.003	0.9962±0.003	0.9964±0.003	0.9950±0.004	0.9964±0.003	0.9907±0.006	0.9823±0.014
	UTV [7]	0.9911±0.002	0.9928±0.002	0.9954±0.002	0.9917±0.007	0.9937±0.004	0.9914±0.005	0.9886±0.019	0.9851±0.012
	GSLV [10]	0.9916±0.007	0.9903±0.008	0.9966±0.008	0.9969±0.005	0.9962±0.010	0.9967±0.008	0.9956±0.009	0.9933±0.015
	LRSID [11]	0.9932±0.004	0.9947±0.003	0.9936±0.004	0.9957±0.003	0.9956±0.007	0.9962±0.004	0.9975±0.009	0.9924±0.040
	Proposed	**0.9994±0.001**	**0.9986±0.001**	**0.9994±0.006**	**0.9986±0.001**	**0.9990±0.001**	**0.9986±0.001**	**0.9979±0.001**	**0.9942±0.004**

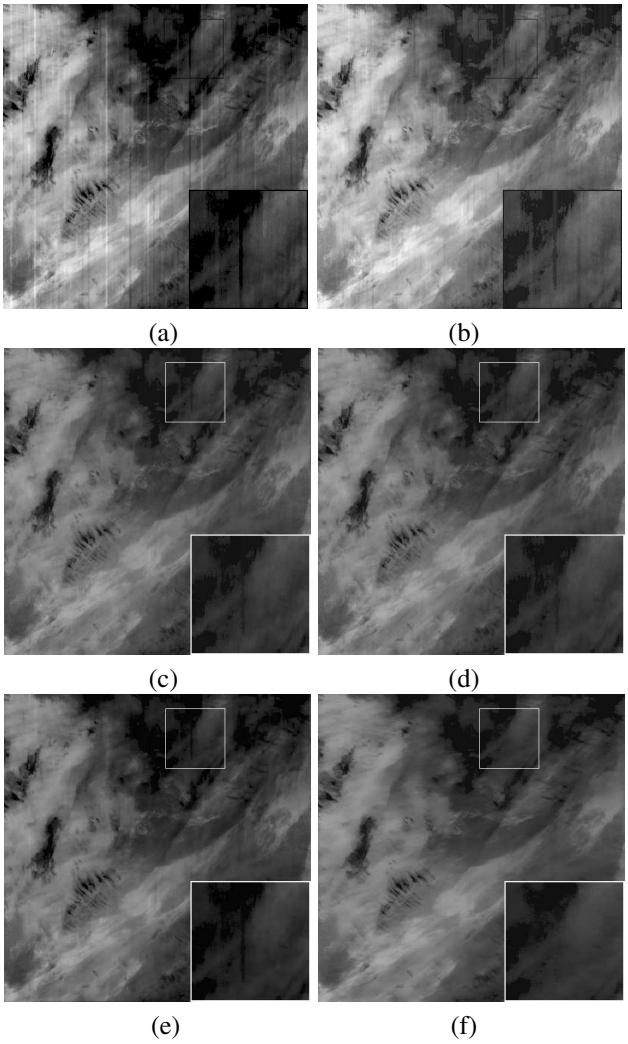

Fig. 1. (a) Remote sensing image with real stripes; (b) SLD; (e) UTV; (f) GSLV; (g) LRSID; (h) Proposed method. Readers are recommended to zoom in all figures for better visibility.

methods can not remove stripes and a little bit change the image structural information. In particular, SLD method shows more bright background information while UTV, GSLV, LRSID and our method all exhibit a little bit dark for the image background. Note that the methods GSLV and LRSID fail to obtain excellent results like their corresponding papers, since they worked for different images with different parameters setting. However, in the experiments, we compare different approaches on 32 remote sensing images with only one parameters setting for each methods, which indicates the stability of our method to the parameters.

4. CONCLUSIONS

In this paper, we proposed a directionally non-convex ℓ_0 sparse model for remote sensing image destriping. This model was solved by a PADMM based algorithm and the MPEC reformulation, which guaranteed the solution converging to the KKT point. Experimental results on simulated and real data demonstrated the effectiveness of the proposed method, both quantitatively and visually. Moreover, the average performance of Table 1 also exhibits the stability of our method to parameters and different remote sensing images with stripes. In the future, we will extend the proposed model to the oblique stripes removal by fully considering the latent properties of oblique stripes.

5. ACKNOWLEDGMENT

This research is supported by 973 Program (2013CB329404), NSFC (61370147, 61402082, 11401081) and the Fundamental Research Funds for the Central Universities (ZYGX2016 KYQD142, ZYGX2016J132, ZYGX2016J129).

6. REFERENCES

[1] H. Carfantan and J. Idier, "Statistical linear destriping of satellite-based pushbroom-type images," *IEEE Transactions on Geoscience and Remote Sensing*, vol. 48, pp. 1860–1871, 2010.

[2] P. Rakwatin, W. Takeuchi, and Y. Yasuoka, "Stripe noise reduction in MODIS data by combining histogram matching with facet filter," *IEEE Transactions on Geoscience and Remote Sensing*, vol. 45, pp. 1844–1856, 2007.

[3] F. L. Gadallah, F. Csillag, and E. J. M. Smith, "Destriping multisensor imagery with moment matching," *International journal of remote sensing*, vol. 21, pp. 2505–2511, 2000.

[4] M. P. Weinreb, R. Xie, J. H. Lienesch, and D. S. Crosby, "Destriping GOES images by matching empirical distribution functions," *Remote Sensing of Environment*, vol. 29, pp. 185–195, 1989.

[5] L. X. Sun, R. Neville, K. Staenz, and H. P. White, "Automatic destriping of Hyperion imagery based on spectral moment matching," *Canadian Journal of Remote Sensing*, vol. 34, pp. S68–S81, 2008.

[6] H. F. Shen and L. P. Zhang, "A MAP-based algorithm for destriping and inpainting of remotely sensed images," *IEEE Transactions on Geoscience and Remote Sensing*, vol. 47, pp. 1492–1502, 2009.

[7] M. Bouali and S. Ladjal, "Toward optimal destriping of MODIS data using a unidirectional variational model," *IEEE Transactions on Geoscience and Remote Sensing*, vol. 49, pp. 2924–2935, 2011.

[8] H. Y. Zhang, W. He, L. P. Zhang, H. F. Shen, and Q. Q. Yuan, "Hyperspectral image restoration using low-rank matrix recovery," *IEEE Transactions on Geoscience and Remote Sensing*, vol. 52, pp. 4729–4743, 2014.

[9] W. He, H. Y. Zhang, L. P. Zhang, and H. F. Shen, "Total-variation-regularized low-rank matrix factorization for hyperspectral image restoration," *IEEE Transactions on Geoscience and Remote Sensing*, vol. 54, pp. 178–188, 2016.

[10] X. X. Liu, X. L. Lu, H. F. Shen, Q. Q. Yuan, Y. L. Jiao, and L. P. Zhang, "Stripe Noise Separation and Removal in Remote Sensing Images by Consideration of the Global Sparsity and Local Variational Properties," *IEEE Transactions on Geoscience and Remote Sensing*, vol. 54, pp. 3049–3060, 2016.

[11] Y. Chang, Yan L. X., T. Wu, and S. Zhong, "Remote Sensing Image Stripe Noise Removal: From Image Decomposition Perspective," *IEEE Transactions on Geoscience and Remote Sensing*, vol. 54, 2016.

[12] G. Z. Yuan and B. Ghanem, "l0TV: A new method for image restoration in the presence of impulse noise," *IEEE Conference on Computer Vision and Pattern Recognition*, pp. 5369–5377, 2015.

[13] X. L. Zhao, F. Wang, and M. K. Ng, "A new convex optimization model for multiplicative noise and blur removal," *SIAM Journal on Imaging Sciences*, vol. 7, pp. 456–475, 2014.

[14] L. J. Deng, H. Guo, and T. Z. Huang, "A fast image recovery algorithm based on splitting deblurring and denoising," *Journal of Computational and Applied Mathematics*, vol. 287, pp. 88–97, 2015.

[15] X.-L. Zhao, W. Wang, T.-Y. Zeng, T.-Z. Huang, and M. K. Ng, "Total variation structured total least squares method for image restoration," *SIAM Journal on Scientific Computing*, vol. 35, no. 6, pp. B1304–B1320, 2013.

[16] J. F. Yang, Y. Zhang, and W. T. Yin, "An efficient TVL1 algorithm for deblurring multichannel images corrupted by impulsive noise," *SIAM Journal on Scientific Computing*, vol. 31, pp. 2842–2865, 2009.

[17] L.-J. Deng, W. Guo, and T.-Z. Huang, "Single image super-resolution via an iterative reproducing kernel Hilbert space method," *IEEE Transactions on Circuits and Systems for Video Technology*, vol. 26, pp. 2001–2014, 2016.

[18] L. J. Deng, W. Guo, and T. Z. Huang, "Single image super-resolution by approximate Heaviside functions," *Information Sciences*, vol. 348, pp. 107–123, 2016.

[19] X. L. Zhao, F. Wang, T. Z. Huang, M. K. Ng, and R. Plemmons, "Deblurring and sparse unmixing for hyperspectral images," *IEEE Trans. Geoscience and Remote Sensing*, vol. 51, pp. 4045–4058, 2013.

[20] D. L. Donoho, "De-noising by soft-thresholding," *IEEE Transactions on Information Theory*, vol. 41, pp. 613–627, 1995.

[21] Z. Wang, A. C. Bovik, H. R. Sheikh, and E. P. Simoncelli, "Image Quality Assesment: From Error Visibility to Structural Similarity," *IEEE Transactions on Image Processing*, vol. 13, pp. 600–612, 2004.